BOLETIN DE LA SOCIEDAD ESPAÑOLA DE
Cerámica y Vidrio
www.elsevier.es/bsecv

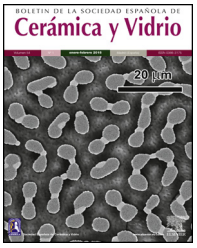

Original

Mechanochemical processing of IrO_2–Ta_2O_5: An alternative route for synthesizing Ir and Ir(Ta)O_2 solid solution

Danny Guzmán[a,*], *Gabriel Dubray*[a], *Claudio Aguilar*[b], *Paula Rojas*[c], *Alexis Guzmán*[a], *Álvaro Soliz*[a], *Rossana Sepúlveda*[a], *Rodrigo Espinoza*[d]

[a] *Departamento de Ingeniería en Metalurgia, Universidad de Atacama, Copiapó, Chile*
[b] *Departamento de Ingeniería en Metalúrgica y de Materiales, Universidad Técnica Federico Santa María, Valparaíso, Chile*
[c] *Escuela de Diseño, Universidad Adolfo Ibáñez, Santiago, Chile*
[d] *Departamento de Ciencia de los Materiales, Universidad de Chile, Santiago, Chile*

ARTICLE INFO

Article history:
Received 19 September 2019
Accepted 29 January 2020
Available online 17 February 2020

Keywords:
Mechanochemical synthesis
Oxides
Thermogravimetry
Catalytic material

ABSTRACT

This paper describes a study exploring milling and subsequent heat treatments of pure IrO_2 and Ta_2O_5 powders. Reactants were milled under Ar atmosphere in a SPEX 8000D mill, with structural, morphological, and compositional characterizations (during milling and after subsequent heat treatments) by X-ray diffraction, energy-dispersive spectroscopy, and transmission electron microscopy. Electrochemical stability of powders was evaluated by open circuit potential (OCP). Results showed that the mechanical energy transferred during this process induces a reaction between IrO_2 and Ta_2O_5, forming metallic Ir and Ir(Ta)O_2 saturated solid solution. The study additionally shows that this reaction can be thermally induced with previous mechanical activation of reactants. Electrochemical evaluations of milled powders immersed in H_2SO_4 solution revealed that OCP shifts negatively with increasing milling time, approaching that of pure Ir at 15 h milling.

Procesamiento mecanoquímico de IrO_2–Ta_2O_5: Una ruta alternativa para sintetizar Ir y solución sólida Ir(Ta)O_2

Palabras clave:
Síntesis mecanoquímica
Óxidos
Termogravimetría
Materiales catalíticos

RESUMEN

Este trabajo describe la molienda y subsecuente tratamiento térmico de polvos de IrO_2 y Ta_2O_5. Los reactantes fueron molidos bajo atmósfera de Ar en un molino SPEX 8000D. Los polvos fueron caracterizados mediante difracción de rayos X, espectroscopía de energía dispersiva de rayos X y microscopia electrónica de transmisión. La estabilidad electroquímica fue evaluada mediante potencial de circuito abierto. Los resultados obtenidos mostraron que

* *Corresponding author.*
E-mail address: danny.guzman@uda.cl (D. Guzmán).
https://doi.org/10.1016/j.bsecv.2020.01.010

la energía mecánica transferida durante el proceso de molienda induce la reacción entre el IrO_2 y Ta_2O_5, formando Ir metálico y una solución sólida saturada $Ir(Ta)O_2$. Adicionalmente, se demostró que esta reacción puede ser térmicamente inducida posterior a una activación mecánica de los reactantes. La evaluación electroquímica de los polvos inmersos en una solución de H_2SO_4, reveló que a medida que el tiempo de molienda aumenta, el potencial de circuito abierto disminuye, hasta alcanzar el potencial presentado por el Ir puro luego de las 15 h de molienda.

Introduction

Dimensionally stable anodes (DSAs), patented by Henry Beer in the sixties [1], are known for their particular electrocatalytic properties useful in electrochemistry as electrodes. Since their first description, many studies have explored various metal oxide mixtures as active coatings over metal substrates. Currently, DSAs in chlorine production are made of Ti rod or expanded metal structure with mixed coating of doped Ru and Ti oxides, which provide high electrocatalytic activity and electrical conductivity [2]. Later developments of DSA in other industries soon arrived: in 1975, Sumitomo Metals and Mining Company reported the use of DSA anodes on a commercial scale for electrowinning nickel and cobalt from chloride electrolytes [3]; that said, most commercial electrowinning processes are with sulfate electrolytes where oxygen-evolving anodes are required. To abate the use of sulfate solutions, RuO_2 was one of the first coatings studied because of its relatively low cost and success in the chloralkali industry; however, it is not stable in the potential range required for oxygen evolution in acid solution [4]. Considerable research has been devoted to formulating mixed coatings with less-expensive metal oxides to prevent or decrease the rate of loss of active material [5–7]. Due to the importance and high demand for materials in these industries, the search for alternatives pointed toward iridium oxide as an electroactive component for oxygen evolution.

To that end, iridium oxide anodes are usually prepared through thermal decomposition of a precursor solution over a Ti substrate at a temperature of 450 °C or more [8]. The research group of professor Comninellis [9,10] established that the best balance of electrocatalytic activity and coating stability is obtained with an oxide composition of IrO_2–30 mol% Ta_2O_5. Similar optimal compositions have been replicated by Mraz and Krysa [11], Xu and Scantlebury [12], Bao-song et al. [13], and Huang et al. [14]. In seeking to explain this optimal balance, Hu et al. [15] systematically studied the effects of oxide composition on phase evolution in IrO_2–Ta_2O_5 coatings. That study found that the high electrochemical performance in Ti/IrO_2–30 mol% Ta_2O_5 anodes are likely due to the formation of a saturated solid solution between IrO_2 and Ta. This conclusion was later confirmed by Yonglei et al. [16].

It is well known that thermal decomposition conditions influence microstructure and electrochemical performance in Ti/IrO_2–Ta_2O_5 anodes. Vercesi et al. [17] studied the effect of calcination temperature on microstructure and electrochemical behavior for these, and found that electrocatalytic activity decreases with as calcination temperature increases. In this same sense, Xu et al. [18] reported that the electrochemical stability of these coatings decreases as calcination temperature decreases. Both these authors [17,18] suggest that this behavior may be related to the degree of crystallinity in the IrO_2 phase.

Additionally, it has been determined that pretreating the Ti substrate affects electrochemical properties in Ti/IrO_2–Ta_2O_5 anodes. Yan et al. [19] compared anodes pretreated with oxalic acid etching vs. those with a hydrogen pretreated substrate, and found that the latter showed greater catalytic activity; however, due to the preferred crystallization orientation of the IrO_2, its lifetime was shorter. Furthermore, Xu et al. [20] found that sandblasting as substrate pretreatment reduced the lifetime of Ti/IrO_2–Ta_2O_5 anodes due to the oxidation of the Ti substrate. In this same sense, Huang et al. [21] studied three Ti pretreatments (grinding with emery paper, HCl etching and NH_4HF_2/HNO_3 etching), finding that the lifetime of Ti/IrO_2–Ta_2O_5 anodes greatly depends on the type of Ti substrate pretreatment.

Other preparation methods have been tested with the objective of improving the electrochemical performance of Ti/IrO_2–Ta_2O_5 anodes. Xu et al. [22] reported that, in comparison with the anodes produced by conventional thermal decomposition, oxide electrodes obtained by the Pechini method exhibited better electrocatalytic activity, likely due to the particular microstructure produced by this synthesis route, which is characterized by a uniform thin film of oxide with high nanoscale roughness. Additionally, Herrada et al. [23] investigated microstructural characteristics and electrochemical behavior of Ti/IrO_2–Ta_2O_5 anodes produced by electrophoretic deposition, concluding that the formation of a homogeneous surface coverage had higher active surface area in comparison with oxide films obtained by thermal decomposition.

Of all the techniques discussed above, a recently published work by Senna [24] provides a comprehensive overview of both theoretical and practical advances in the field of Mechanochemistry. The branch of chemistry concerned with chemical and physicochemical transformations of substances in all states of aggregation through mechanical energy [25]. Mechanochemistry looks to be a highly promising and simple means of obtaining materials which are very complicated to synthesize by other routes [26–29]. Significantly, mechanochemistry induces phase transformations where crystalline defects play an important role in increasing the rate of solid state reactions. Here, such processes (e.g., mechanical alloying and milling) increase the number and density of

crystalline defects, which could be an alternative in the manufacture of special purpose materials – including Ir(Ta)O_2 solid solutions – even as it continues to be developed for hydrogen storage materials [30].

Despite the importance of saturated Ir(Ta)O_2 solid solutions in improving electrochemical performance in Ti/IrO_2–Ta_2O_5 anodes [15,16], no works as yet have determined the possibility of obtaining a supersaturated Ir(Ta)O_2 solid solution. This oversight is not irrelevant, given that higher Ta content in oxide coatings would reduce manufacturing costs and increase electrochemical stability in this type of anode.

Based on the above, then, the objective of the present work was to study the milling and subsequent heat treatment of IrO_2 and Ta_2O_5 powders in order to synthesize a Ta-supersaturated Ir(Ta)O_2 solid solution. The effects of milling time and heat treatment on the microstructural and electrochemical properties of the powders obtained were also investigated.

Experimental procedures

Milling

IrO_2 (99.9% purity, Sigma Aldrich) and Ta_2O_5 (99.0% purity, Sigma Aldrich) powders were milled at ratio of IrO_2 38 mol% Ta_2O_5 in a SPEX 8000D mill under Ar atmosphere (10 ppm of O_2) using a ball-to-powder ratio (BPR) of 10–1. This BPR is quite common in similar materials, and hence selected in this study. To prevent excessive welding during mechanochemical processes, 1 wt.% stearic acid was added as a processing control agent. Milling times were 1, 3, 5, 10, and 15 h. To minimize temperature rise during milling, this process was performed discontinuously, i.e., 0.5 h of milling followed by rest periods of 0.5 h.

Microstructural and morphological characterization

The microstructural evolution of the powders during the mechanochemical process was studied by X-ray diffraction (XRD) in a Shimadzu XDR-6000 diffractometer using Cu-Kα radiation. The XRD analyses were carried out using an angular step of 0.02° (2θ) and a counting time per step of 6 s. XRD patterns were analyzed with the Rietveld method [31] in the Materials Analysis Using Diffraction (MAUD) program [32]. Powder morphology was evaluated using a Zeiss EVO MA 10 thermionic scanning electron microscope (SEM). Additionally, powder microstructure was analyzed by transmission electron microscopy (TEM) using a FEI Tecnai F20 ST microscope.

Thermal characterization

Thermal behavior of the mechanically alloyed powder was determined through a combination of simultaneous differential scanning calorimetry (DSC) and thermogravimetric analyses (TGA) (SDT 650, TA Instruments). The thermal analyses were carried out under an Ar flow of 50 mL min^{-1}, and samples were heated from room temperature to 1300 °C at a heating rate of 20 °C min^{-1}.

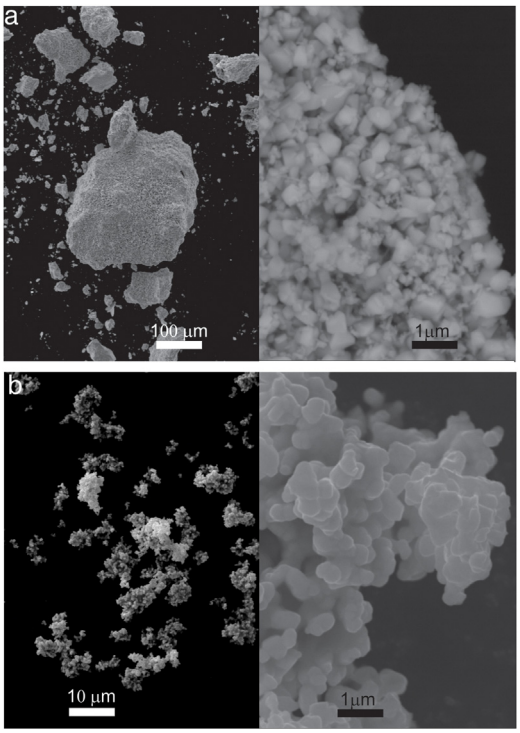

Fig. 1 – Morphology and particle size of raw powders: (a) IrO_2 and (b) Ta_2O_5.

Electrochemical characterization

Electrochemical characterization of powders was performed on a modified carbon electrode immersed in an aerated 1.63 M H_2SO_4 solution. This concentration was chosen because it is the typical acid concentration in the Cu electrowinning, where Ti/IrO_2–Ta_2O_5 DSA anodes are commonly used. Working electrodes were prepared with 0.25 g of the sample and 0.25 g of graphite powders, mixed with 0.33 g of paraffin wax at 70 °C. This mixture was then placed into a Teflon tube with an internal diameter of 3 mm, and copper wire was used to ensure electrical contact. Electrochemical measurements were carried out in a conventional three-electrode cell with Ag/AgCl (sat. KCl) and platinum wires as reference and counter electrodes, respectively. Open circuit potential (OCP) was performed at room temperature (22 ± 0.5 °C) using a BioLogic (VSP-300) potentiostat/galvanostat. To determine the OCP for each sample, the working electrode was maintained in the test solution for 15 h. The concentration of the elements dissolved was determined after each electrochemical test by inductively coupled plasma spectrometry (ICP) using Perkin Elmer Optima 8000 equipment.

Results and discussion

Powders were characterized by particle size (granulometry) and particle shape (morphology). Fig. 1 shows SEM images of raw materials used in the milling process. Both samples formed from fine particle agglomerates. The calculated average particle sizes for IrO_2 and Ta_2O_5 were 330 ± 30 and

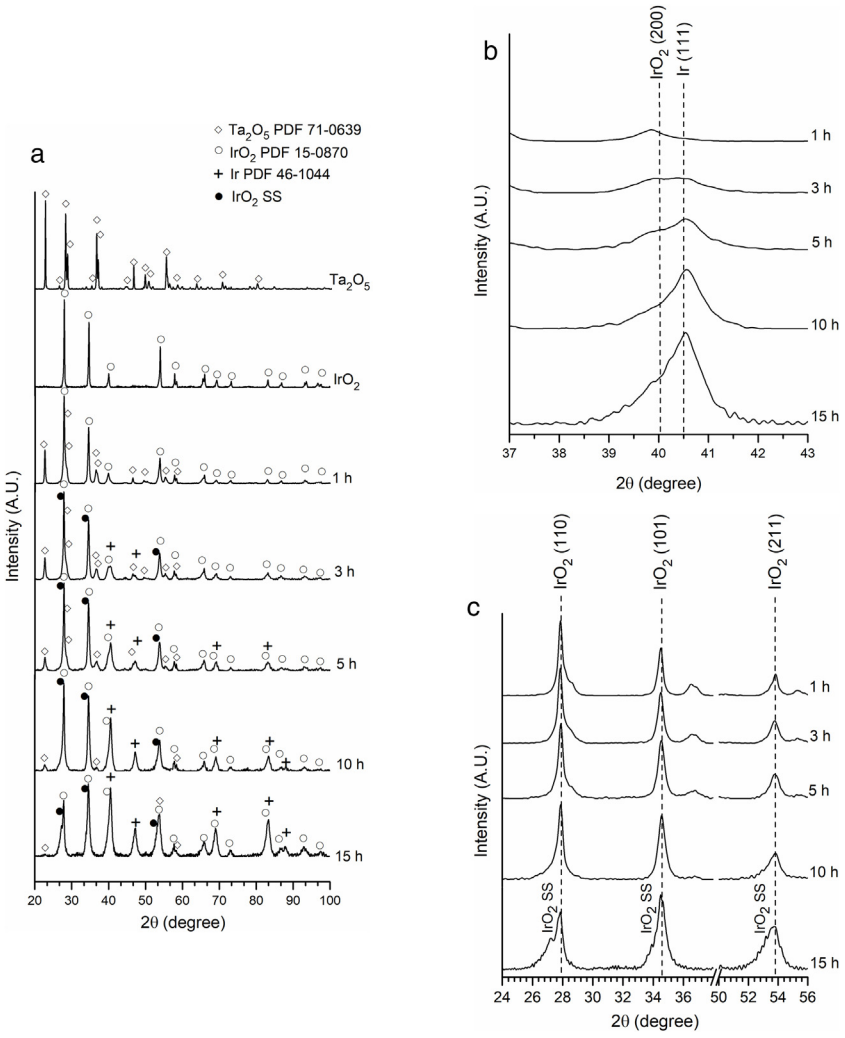

Fig. 2 – (a) XRD patterns of initial reactants and powders after 1, 3, 5, 10, and 15 h of milling; (b) and (c) are magnifications of selected areas.

532 ± 37 nm, respectively. In terms of morphology, IrO_2 presented particles with sharp edges, whereas the Ta_2O_5 sample exhibited particles with smoother, more rounded edges.

The XRD patterns of the pure compounds are shown in Fig. 2(a) together with XRD patterns of the phases after milling. The microstructural information was obtained from Rietveld refinements. The results for oxides before milling are listed in Table 1. The refined lattice parameters for IrO_2 and Ta_2O_5 are in agreement with those reported in literature for tetragonal IrO_2 ($a = 0.4498$ nm, $c = 0.3154$ nm) [33] and orthorhombic Ta_2O_5 ($a = 0.6198$ nm, $b = 4.0290$ nm, and $c = 0.3888$ nm) [34]. Additionally, Ta_2O_5 exhibits a larger average crystallite size than IrO_2, related to the difference of initial particle size between these two oxides [35].

Fig. 2 shows the XRD patterns of initial reactants and powders after 1, 3, 5, 10, and 15 h of milling. To compare the XRD patterns, they were normalized with respect to the maximum intensity. The corresponding fitting and crystalline parameters are listed in Table 2.

After the first hour of milling, only IrO_2 and Ta_2O_5 were detected. During this milling period, the unit cell volume of both oxides remained practically unchanged in comparison with the raw materials.

After 3 h of mechanochemical processing, the relative peak intensity of Ta_2O_5 gradually decreases. Only traces of this compound were found after 15 h of milling. No appreciable change of the Ta_2O_5 unit cell volume was detected, which dismisses the formation of a solid solution based on this oxide during the mechanochemical process. Additionally, it was possible to detect diffraction peaks of metallic Ir, whose relative intensity gradually increases with milling time (Fig. 2(b)). The refined unit cell volume for metallic Ir (56.56×10^{-3} nm^3 in average, Table 2) is in agreement with reports in the literature by Kern and Eysel [36].

As can be seen in Fig. 2(c), the IrO_2 diffraction peaks become more asymmetric as milling time increases. Finally, after 15 h of milling, a new set of peaks can be clearly distinguished to the left of the original IrO_2 diffraction peaks. These additional peaks can be attributed to the formation of a new phase which possesses the same structure type as the tetragonal IrO_2 but with a larger lattice unit volume. Fig. 3 presents the refined lattice parameters of this new phase at the different milling

Table 1 – Microstructural and fitting parameters obtained from the Rietveld method for IrO_2 and Ta_2O_5 before milling.

	Space group	Lattice parameters (nm)			Unit cell volume (nm³) × 10^{-3}	Crystallite size (nm)	R_B (%)	χ^2 (%)
		a	*b*	*c*				
IrO_2	$P4_2/mnm$	0.4500		0.3157	63.92	58	8.50	1.36
Ta_2O_5	C2mm	0.6197	4.0282	0.3889	970.82	185	7.61	2.70

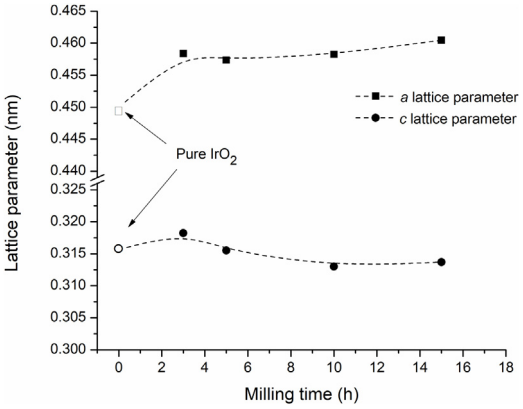

Fig. 3 – Lattice parameters of IrO_2 solid solution over mechanochemical processing.

times. In comparison with initial IrO_2, the new phase shows a large "*a*" parameter. No appreciable changes in "*c*" parameter were observed. Similar results were reported by Roginskaya et al. [37], who studied the formation of IrO_2–Ta_2O_5 film by thermal decomposition. They found that the substitution of Ir IV (radius 0.71 pm) by Ta IV cations (radius 0.74 pm) into IrO_2 structure results principally in an expansion of the "*a*" lattice parameter.

The detection of this new phase, taken with the decreased Ta_2O_5 relative peak intensity and the changes in the crystalline parameters mentioned above, suggest the formation of an $Ir(Ta)O_2$ solid solution (IrO_2 SS) through mechanochemical processing. To corroborate this assumption, powders milled after 15 h were subjected to TEM and analyzed with energy-dispersive X-ray spectroscopy (EDS). The results obtained are shown in Fig. 4, with a sample composed of nanometric particle agglomerates. The selected area electron diffraction (SAED) shows defined rings, characteristic of polycrystalline materials. Furthermore, punctual EDS analyses revealed particles with high Ir, Ta, and O content. It is important to note that detected Cu originated from the TEM grid support, while Fe comes from the erosion of the balls used in milling. Considering that only traces of Ta_2O_5 were founded after 15 h of milling and that no amorphous phases were found by XRD and TEM, it is possible to conclude that the increase in the density of crystalline defects generated by milling, caused the formation of a $Ir(Ta)O_2$ solid solution.

The unit cell volume of the $Ir(Ta)O_2$ solid solution does not vary appreciably with milling time (Table 2), suggesting that this phase is not produced by a gradual diffusion of Ta into IrO_2, but is rather the result of a chemical reaction between IrO_2 and Ta_2O_5. On the other hand, the cell volume average of the $Ir(Ta)O_2$ solid solution formed during milling (66.3×10^{-3} nm³) is very close to that of reports by Hu et al. (66.6×10^{-3} nm³) [15,38] and Yonglei (66.0×10^{-3} nm³) [16] for a saturated solid solution. This evidence indicates that, under the experimental conditions employed, it was not possible to form a supersaturated $Ir(Ta)O_2$ solid solution. This conclusion is further supported by XRD analysis of powders milled after 15 h, where traces of Ta_2O_5 can still be detected (Fig. 2(a)).

Fig. 5 presents the evolution of average crystallite size and microstrains as a function of milling time for IrO_2 and Ta_2O_5. Crystallite size significantly decreases for both oxides during the first hours of milling; indeed, ceramics subjected to milling have been shown to very quickly undergo brittle fracture as a result of pre-existing defects [39]. After 3 h, the crystallite size reaches a saturation value of 34 nm for IrO_2 and 16 nm for Ta_2O_5. The results obtained suggest that under the experimental conditions employed, both oxides reached their "comminution limit", below which crack propagation is impossible [40–42]. Considering that the calculated microstrain is very low for both oxides (Fig. 5), it is possible to conclude that the crystallite size refinement during milling occurs via repeated brittle fracture and not by severe plastic deformation. The fact that the final crystallite size obtained by XRD and the particle size determined

Table 2 – Microstructural and fitting parameters obtained from the Rietveld method for the milled powders.

Time (h)	Unit cell volume (nm³) × 10^{-3}				Wt% Ir[a]	R_B (%)	χ^2 (%)
	IrO_2	IrO_2 SS	Ta_2O_5	Ir			
1	64.14	–	976.05	–	–	8.80	1.71
3	64.23	66.87	979.61	56.52	5.6	7.52	1.33
5	64.25	66.00	977.90	56.67	15.2	6.38	1.23
10	64.12	65.73	972.58	56.50	20.3	5.53	1.16
15	64.01	66.38	–	56.54	23.4	5.41	1.55

Note: [a]The Ir concentration is only referential because the powders were positioned on a glass sample holder, whose signal interferes with the precise quantification of the phases by XRD.

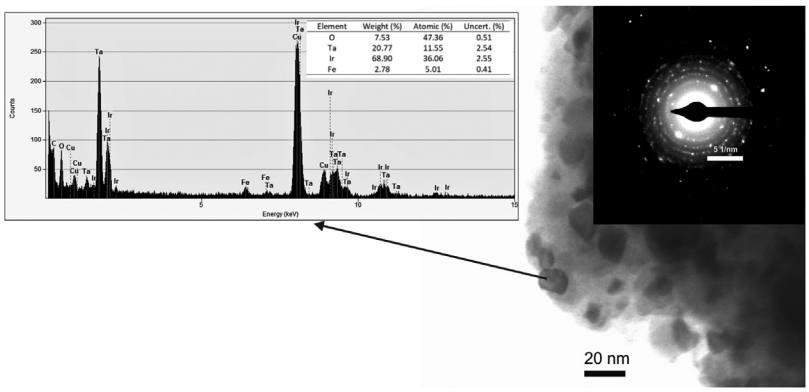

Fig. 4 – TEM, SAED, and EDS of powders after 15 h milling.

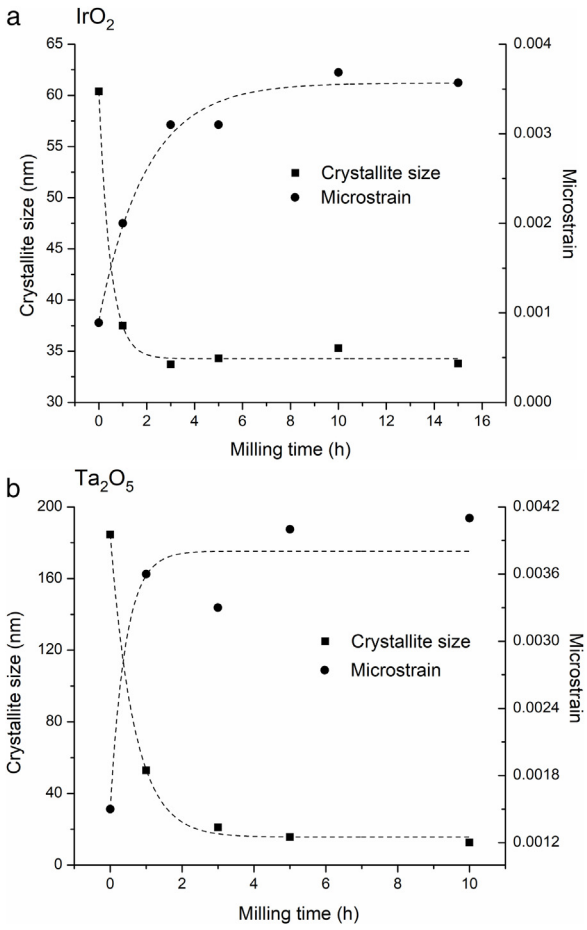

Fig. 5 – Calculated crystallite size and microstrain as a function of milling time for (a) IrO_2 and (b) Ta_2O_5.

by TEM (Fig. 4) are in the same range demonstrates that the particles are single crystals and corroborates that brittle fracture is the dominant mode of microstructure refinement.

The dissociation of IrO_2, given by Eq. (1), is not a spontaneous process under normal conditions. The Gibbs free energy change for this reaction at 298 K and a partial O_2 pressure of 1×10^{-5} atm (O_2 content in commercial Ar) is 164.33 kJ mol^{-1} [43].

$$IrO_2 \rightarrow Ir + O_2 \quad (g) \tag{1}$$

During mechanochemical processes, it is well known that a part of the energy is retained by the solid in the form of new surface and lattice defects [44]. These increases in the internal energy of the reactants in some cases can induce non-spontaneous processes during the milling [45,46].

Considering the low microstrain calculated for milled IrO_2 (Fig. 5), it is possible to establish that newly formed surface areas are the main contribution to free energy changes during mechanochemical processing. Thus, for dissociation of IrO_2 by Eq. (1) to be spontaneous under the milling conditions employed, the energy contribution of the surface due to the decrease in the particle size of IrO_2 must be greater than 164.33 kJ mol^{-1}. In order to obtain an approximation of the free energy increase of IrO_2 due to the milling process, we assumed spherical particles of 34 nm in diameter. The surface energy of this oxide (2.16 J m^2) was taken from Ref. [47]. The results obtained suggest that the free energy increases due to the formation of new surfaces (7.33 kJ mol^{-1}) is insufficient to promote the decomposition of IrO_2 in Ir and O_2.

As mentioned earlier, the formation of $Ir(Ta)O_2$ solid solutions has been previously reported by several authors under thermal decomposition of chloride precursors [13–16,18,38]. Hu et al. determined that this phase has a high thermal stability, finding that when this solid solution is heated to 800 °C in air, decomposition into elemental oxides (IrO_2 and Ta_2O_5) does not take place [38].

Based on the results obtained and considering the high thermal stability of $Ir(Ta)O_2$ solid solutions, it is proposed that the decomposition of IrO_2 during milling is very likely due to two factors: (i) the energy transferred to the powders from the production of new surfaces; and (ii) the formation of a stable $Ir(Ta)O_2$ saturated solid solution, which would reduce the Gibbs free energy of the products and allow for its decomposition under the conditions employed, according to Eq. (2):

$$IrO_2 + \frac{x}{2}Ta_2O_5 = xIr + Ir_{1-x}(Ta_x)O_2 + \frac{5x}{4}O_2 \quad (g) \tag{2}$$

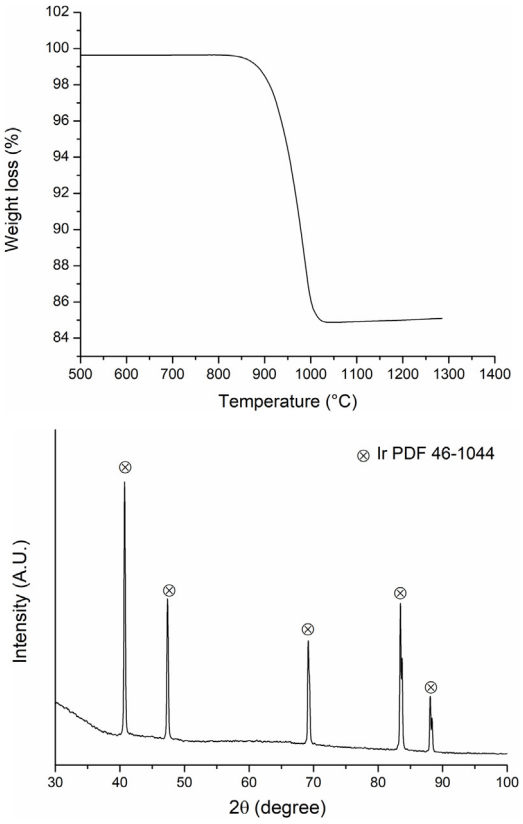

Fig. 6 – (a) TGA curve for initial IrO_2 powder and (b) XRD pattern of the same sample after heat treatment.

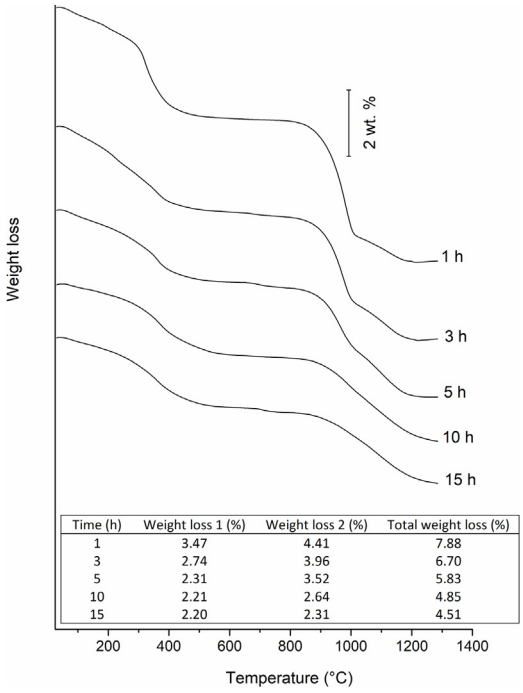

Time (h)	Weight loss 1 (%)	Weight loss 2 (%)	Total weight loss (%)
1	3.47	4.41	7.88
3	2.74	3.96	6.70
5	2.31	3.52	5.83
10	2.21	2.64	4.85
15	2.20	2.31	4.51

Fig. 7 – TGA curves of powders after 1, 3, 5, 10, and 15 h milling.

Thermal stability of the powders after milling was analyzed by DSC/TGA and XRD. Fig. 6(a) shows the thermogravimetric analysis for initial IrO_2 powders. A 15% weight loss occurs from 810 to 1030 °C, i.e., thermal decomposition of IrO_2 according to reaction (1). The presence of metallic Ir after heat treatment was confirmed by XRD (Fig. 6(b)). In relation to Ta_2O_5, no reactions were detected during heating.

Fig. 7 shows TGA curves of powders at 1, 3, 5, 10, and 15 h milling. Two stages of weight loss can be observed during heating. To determine the nature of these stages, powders milled during 1 h were heated up to 600 °C and 1300 °C and analyzed by XRD. The results can be seen in Fig. 8.

In contrast to the powders at 1 h milling, the X-ray pattern for powders heated to 600 °C shows the presence of Ir and $Ir(Ta)O_2$. Based on the results obtained, it is possible to conclude that the weight loss between 25 and 600 °C can be attributed to the reaction between mechanically activated IrO_2 and Ta_2O_5 powders according to Eq. (2).

Concerning the sample heated to 1300 °C, the X-ray pattern showed the presence of Ta_2O_5, Ir, $FeTa_2O_6$, and TaO_2. Considering the results obtained, the weight loss between 810 and 1030 °C is principally associated with the thermal decomposition of the remaining IrO_2 and the $Ir(Ta)O_2$ solid solution. The formation of $FeTa_2O_6$ is due to the reaction between Ta

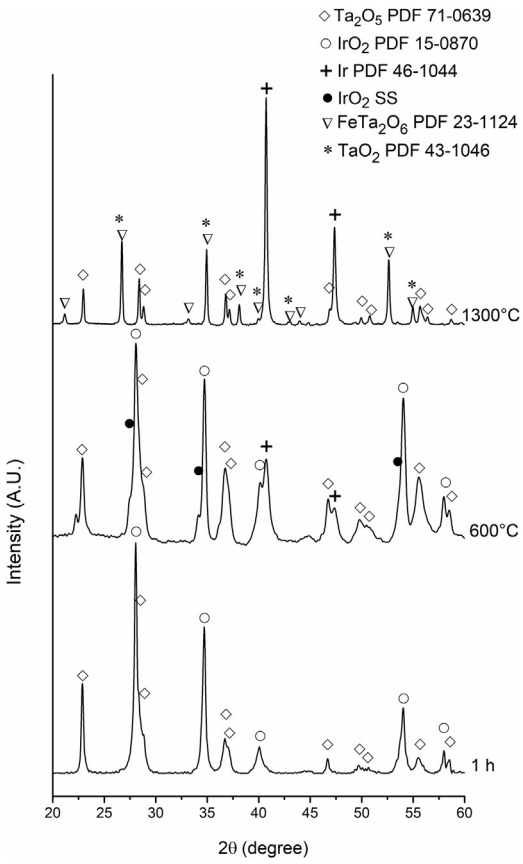

Fig. 8 – XRD patterns of samples milled for 1 h and heated up to 600 and 1300 °C.

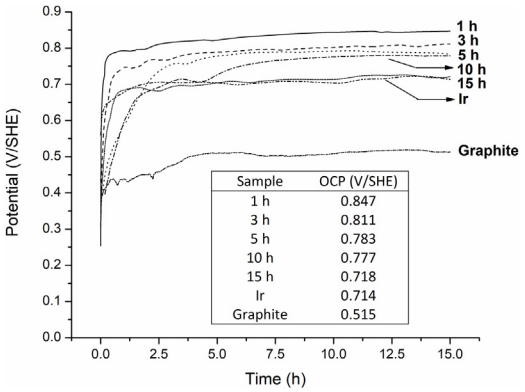

Fig. 9 – OCP measurements in 1.63 M H_2SO_4 solution for graphite, pure Ir and IrO_2-Ta_2O_5 powders at different milling times.

released during the decomposition of the Ir(Ta)O_2 solid solution and Fe from balls used in milling.

The table insert in Fig. 7 shows that weight loss under these two reactions decreases with milling time. Considering that Eq. (2) can be mechanically or thermally induced, as milling progresses, lesser amount of IrO_2 will be available for thermal decomposition.

Finally, Fig. 9 shows OCP variations, as a function of milling time, in a 1.63 M H_2SO_4 solution at 22 °C. The OCP for graphite and pure Ir are presented for comparison. It is possible to observe that the graphite electrode showed the lowest OCP value suggesting that the potential of the IrO_2–Ta_2O_5 electrodes is being dominated by the processes occurring on the milled powders instead of graphite surface. Additionally, it is noted that the steady state OCP shifts negatively with increasing milling time, approaching that of pure Ir. In concordance with the XRD results shown in Fig. 2, this behavior confirms that milling generates metallic Ir following Eq. (2). The Pourbaix diagram of Ir [48] at bulk pH of 0.5 shows that all measured OCP values lay in the immunity domain, providing evidence for the presence of this metal in the milled powders. The high stability of the milled powders, composed principally of metallic Ir and Ir(Ta)O_2 solid solution was corroborated by chemical analysis using ICP spectroscopy in a concentrated H_2SO_4 solution. In all cases Ir and Ta concentrations in solution, measured after the OCP tests, were below the detection limit of the equipment used ([Ir] < 0.01 mg L^{-1} and [Ta] < 0.015 mg L^{-1}). On the other hand, Fe concentration fluctuated between 0.65 and 0.87 mg L^{-1}, for the powders with 1 and 15 h of milling. This result indicates that, although there is a contamination by Fe during the mechanochemical processing, this contamination does not intensify excessively with the increase of the milling time.

Conclusions

Concerning the phase evolution of powders during milling, it is possible to conclude that the mechanical energy transferred induces a reaction between IrO_2 and Ta_2O_5, forming metallic Ir and an Ir(Ta)O_2 saturated solid solution. The study additionally shows that this reaction can be thermally induced with previous mechanical activation of reactants.

The non-formation of an supersaturated Ir(Ta)O_2 solid solution during milling is due to above phase evolution, which, rather than a continuous diffusion of Ta into the IrO_2 structure, is a solid-state reaction between mechanically activated IrO_2 and Ta_2O_5.

Finally, variations in OCP of the powders over milling times revealed high stability against further oxidation, which as also validated by chemical analysis.

Acknowledgments

This study was financially supported by FONDECYT [Project No. 1151204]. The authors wish to thank the Metallurgy Department of University of Atacama for the XRD, SEM, and DSC analyses [Projects EQM 130125, EQUV 003, and EQUR 16002]. Additionally, Gabriel Dubray thanks to the University of Atacama for the postgraduate fellowship.

REFERENCES

[1] M. Nuñez, Trends in Electrochemistry, Nova Science Publishers, New York, 2007.
[2] P. Duby, The history of progress in dimensionally stable anodes, JOM-J. Min. Met. Mater. Sci. 45 (1993) 41–43, http://dx.doi.org/10.1007/BF03222350.
[3] T. Åkre, Electrowinning of cobalt from chloride solutions: anodic deposition of cobalt oxide on DSA, Ph.D. Thesis, Tapir Uttrykk, Trondheim, Norway, 2008.
[4] C. Vallet, S. Borns, J. Hendrickson, C. White, DSA RuO_2/TiO_2 electrode modeled by ion implantation: an in-situ characterization by photo-acoustic and photocurrent spectroscopy, J. Electrochem. Soc. 135 (1988) 387–395, http://dx.doi.org/10.1149/1.2095622.
[5] R. Otogawa, M. Morimitsu, M. Matsunaga, Effects of microstructure of IrO_2-based anodes on electrocatalytic properties, Electrochem. Acta 44 (1998) 1509–1513, http://dx.doi.org/10.1016/S0013-4686(98)00274-6.
[6] L. Vazquez-Gomez, S. Ferro, A. De Battisti, Preparation and characterization of RuO_2–IrO_2–SnO_2 ternary mixtures for advanced electrochemical technology, Appl. Catal. B: Environ. 67 (2006) 34–40, http://dx.doi.org/10.1016/j.apcatb.2006.03.023.
[7] Y. Liu, C. Wang, Y. Lei, F. Liu, B. Tian, J. Wang, Investigation of high-performance IrO_2 electrocatalysts prepared by Adams method, Int. J. Hydrogen Energy 43 (2018) 19460–19467, http://dx.doi.org/10.1016/j.ijhydene.2018.08.196.
[8] W. Zhang, E. Ghali, G. Houlach, Review of oxide coated catalytic titanium anodes performance for metal electrowinning, Hydrometallurgy 169 (2017) 456–467, http://dx.doi.org/10.1016/j.hydromet.2017.02.014.
[9] J. Rolewicz, C. Comninellis, J. Hinden, Charactérisation des électrodes de type DSA pour le dégagement de O_2. L'électrode Ti/IrO_2–Ta_2O_5, Electrochim. Acta 33 (1988) 573–580, http://dx.doi.org/10.1016/0013-4686(88)80180-4.
[10] C. Comninellis, G. Versesi, Characterization of DSA®-type oxygen evolving electrodes: choice of a coating, J. Appl. Electrochem. 21 (1991) 335–345, http://dx.doi.org/10.1007/BF01020219.

[11] R. Mráz, J. Krysa, Long service life IrO_2/Ta_2O_5 electrodes for electroflotation, J. Appl. Electrochem. 24 (1994) 1262–1266, http://dx.doi.org/10.1007/BF00249891.
[12] L. Xu, J. Scantlebury, Microstructure and electrochemical properties of IrO_2–Ta_2O_5-coated titanium anodes, J. Electrochem. Soc. 150 (2003) B254–B261, http://dx.doi.org/10.1149/1.1569479.
[13] L. Bao-song, L. An, G. Fu-Xing, Preparation and electrocataytic properties of Ti/IrO_2–Ta_2O_5 anodes for oxygen evolution, Trans. Nonferrous Met. Soc. China 16 (2006) 1193–1199, http://dx.doi.org/10.1016/S1003-6326(06)60400-7.
[14] C. Huang, S. Yang, P. Lai, Effect of precursor baking on the electrochemical properties of IrO_2–Ta_2O_5/Ti anodes, Surf. Coat. Technol. 25 (2018) 896–903, http://dx.doi.org/10.1016/j.surfcoat.2018.03.095.
[15] J. Hu, J. Zhang, H. Meng, C. Cao, Microstructure, electrochemical surface and electrocatalytic properties of $IrO_2 + Ta_2O_5$ oxide electrodes, J. Mater. Sci. 38 (2003) 705–712, http://dx.doi.org/10.1023/A: 1021840426997.
[16] X. Yonglei, X. Likun, W. Juntao, L. Xiangbo, Effect of sintering temperature on microstructure and electrocatalytic properties of Ti/IrO_2–Ta_2O_5 anodes by Pechini method, Rare Met. Mater. Eng. 39 (2010) 1903–1907, http://dx.doi.org/10.1016/S1875-5372(10)60135-X.
[17] G. Vercesi, J. Salamin, C. Comninellis, Morphological and microstructural study of the Ti/IrO_2–Ta_2O_5 electrode: effect of the preparation temperature, Electrochim. Acta 36 (1991) 991–998, http://dx.doi.org/10.1016/0013-4686(91)85306-R.
[18] W. Xu, G. Haarberg, S. Sunde, F. Seland, A. Ratvik, E. Zimmerman, T. Shimamune, J. Gustavsson, T. Åkre, Calcination temperature dependent catalytic activity and stability of IrO_2–Ta_2O_5 anodes for oxygen evolution reaction in aqueous sulfate electrolytes, J. Electrochem. Soc. 164 (2017) F895–F900, http://dx.doi.org/10.1149/2.0061710jes.
[19] Z. Yan, Y. Zhao, Z. Zhang, G. Li, H. Li, J. Wang, Z. Feng, M. Tang, X. Yuan, R. Zhang, Y. Du, A study on the performance of IrO_2–Ta_2O_5 coated anodes with surface treated Ti substrates, Electrochim. Acta 345 (2015) 345–350, http://dx.doi.org/10.1016/j.electacta.2015.01.005.
[20] W. Xu, G. Haarberg, S. Sunde, F. Seland, A. Ratvik, S. Holmin, J. Gustavsson, Å. Afvander, E. Zimmerman, T. Åkre, Sandblasting effect on performance and durability of Ti based IrO_2–Ta_2O_5 anode in acid solutions, Electrochim. Acta 295 (2019) 204–214, http://dx.doi.org/10.1016/j.electacta.2018.10.144.
[21] C. Huang, S. Yang, C. Chen, F. Hsu, Electrochemical behavior of IrO_2–Ta_2O_5/Ti anodes prepared with different surface pretreatments of Ti substrate, Surf. Coat. Technol. 320 (2017) 270–278, http://dx.doi.org/10.1016/j.surfcoat.2017.01.005.
[22] L. Xu, Y. Xin, J. Wang, A comparative study on IrO_2–Ta_2O_5 coated titanium electrodes prepared with different methods, Electrochim. Acta 54 (2009) 1820–1825, http://dx.doi.org/10.1016/j.electacta.2008.10.004.
[23] R. Herrada, G. Acosta-Santoyo, S. Sepúlveda-Guzmán, E. Brillas, I. Sirés, E. Bustos, IrO_2–Ta_2O_5/Ti electrodes prepared by electrodeposition from different Ir:Ta ratios for the degradation of polycyclic aromatic hydrocarbons, Electrochim. Acta 263 (2018) 353–361, http://dx.doi.org/10.1016/j.electacta.2018.01.056.
[24] M. Senna, How can we make solids more reactive? Basics of mechanochemistry and recent new insights, Chem. Texts 3 (2017) 4, http://dx.doi.org/10.1007/s40828-017-0041-0.
[25] G. Heinicke, Tribochemistry, Akademie–Verlag, Berlin, 1984.
[26] D. Guzmán, C. Aguilar, P. Rojas, J.M. Criado, M.J. Diánez, R. Espinoza, A. Guzmán, C. Martínez, Production of Ag–ZnO powders by hot mechanochemical processing, T. Nonferr. Met. Soc. China 29 (2019) 365–373, http://dx.doi.org/10.1016/S1003-6326(19)64946-0.
[27] C. Ruiz-Aguilara, U. Olivares-Pinto, E.A. Aguilar-Reyes, R. López-Juárez, I. Alfonso, Characterization of β-tricalcium phosphate powders synthesized by sol–gel and mechanosynthesis, Bol. Soc. Esp. Ceram. Vidr. 57 (2018) 213–220, http://dx.doi.org/10.1016/j.bsecv.2018.04.004.
[28] J. Gilabert, M. Palacios, V. Sanz, S. Mestre, Fuel effect on solution combustion synthesis of $Co(Cr,Al)_2O_4$ pigments, Bol. Soc. Esp. Ceram. Vidr. 56 (2017) 215–225, http://dx.doi.org/10.1016/j.bsecv.2017.03.003.
[29] O. Shpotyuk, Z. Bujňáková, M.J. Sayagués, P. Baláž, A. Ingram, Y. Shpotyuk, P. Demchenko, Microstructure characterization of multifunctional As_4S_4/Fe_3O_4 nanocomposites prepared by high-energy mechanical milling, Mater. Charact. 132 (2017) 303–311, http://dx.doi.org/10.1016/j.matchar.2017.08.028.
[30] J. Huot, D. Ravnsbæk, J. Zhang, F. Cuevas, M. Latroche, T. Jensen, Mechanochemical synthesis of hydrogen storage materials, Prog. Mater. Sci. 58 (2013) 30–75, http://dx.doi.org/10.1016/j.pmatsci.2012.07.001.
[31] H. Rietveld, A profile refinement method for nuclear and magnetic structures, J. Appl. Crystallogr. 2 (1969) 65–71, http://dx.doi.org/10.1107/S0021889869006558.
[32] L. Lutterotti, MAUD—Materials Analysis Using Diffraction. Information on http://maud.radiographema.eu/. (accessed 09.04.19).
[33] H. Swanson, M. Morris, E. Evans, Standard X-ray Diffraction Powder Patterns, Monograph 25, Section 4, National Bureau of Standards, Washington, 1966.
[34] Y. Stephenson, R. Roth, Structural systematics in the binary system Ta_2O_5–WO_3. V. The structure of the low-temperature form of tantalum oxide L-Ta_2O_5, Acta Crystallogr. B 27 (1971) 1037–1044, http://dx.doi.org/10.1107/S342X 056774087100.
[35] Q. Li, C. Kartikowati, S. Horie, T. Ogi, T. Iwaki, K. Okuyama, Correlation between particle size/domain structure and magnetic properties of highly crystalline Fe_3O_4 nanoparticles, Sci. Rep-UK 7 (2017) 9894, http://dx.doi.org/10.1038/s41598-017-09897-5.
[36] A. Kern, W. Eysel, Mineralogisch-Petrograph Institut, ICDD Grant-in-Aid, University Heidelberg, Germany, 1993.
[37] Y. Roginskaya, O. Morozova, E. Loubnin, A. Popov, Y. Ulitina, V. Zhurov, S. Trasatti, X-ray diffraction, transmission electron microscopy and X-ray photoelectron spectroscopic characterization of $IrO_2 + Ta_2O_5$ films, J. Chem. Soc., Faraday Trans. 89 (1993) 1707–1715, http://dx.doi.org/10.1039/FT 07 99389017.
[38] J. Hu, J. Zhang, C. Cao, Thermolytic formation and microstructure of $IrO_2 + Ta_2O_5$ mixed oxide anodes from chloride precursors, Thermochim. Acta 403 (2003) 257–266, http://dx.doi.org/10.1016/S0040-6031(03)00061-3.
[39] R. Davis, B. McDermott, C. Koch, Mechanical alloying of brittle materials, Metall. Trans. A 19 (1988) 2867–2874, http://dx.doi.org/10.1007/BF 02647712.
[40] K. Kendall, The impossibility of comminuting small particles by compression, Nature 272 (1978) 710–711, http://dx.doi.org/10.1038/27 0 2710.
[41] J. Hagan, Impossibility of fragmenting small particles: brittle-ductile transition, J. Mater. Sci. 16 (1981) 2909–2911, http://dx.doi.org/10.1007/BF02402857.
[42] J. Field, M. Farhat, S. Walley, Comminution limit (CL) of particles and possible implications for pumped storage reservoirs, J. Mater. Sci. 49 (2014) 3780–3784, http://dx.doi.org/10.1007/s10853-014-8089-3.
[43] E. Cordfunke, The enthalpy of formation of IrO_2 and thermodynamic functions, Termochim. Acta 50 (1981) 177–185, http://dx.doi.org/10.1016/0040-6031(81)85053-8.
[44] P. Baláž, Mechanochemistry in Nanoscience and Minerals Engineering, Springer-Verlag, Berlin, 2008.
[45] N. Al-Aqeeli, M. Hussein, C. Suryanarayana, Phase evolution during high energy ball milling of immiscible Nb–Zr alloys,

Adv. Powder Technol. 26 (2015) 385–391, http://dx.doi.org/10.1016/j.apt.2014.11.008.
[46] M. Molaei, A. Ataie, S. Raygan, S. Picken, E. Mendes, F. Tichelaar, Synthesis and characterization of $BaFe_{12}O_{19}/Fe_3O_4$ and $BaFe_{12}O_{19}/Fe/Fe_3O_4$ magnetic nano-composites, Powder Technol. 221 (2012) 292–295, http://dx.doi.org/10.1016/j.powtec.2012.01.015.
[47] O. Matz, M. Calatayud, Periodic DFT study of rutile IrO_2: surface reactivity and catechol adsorption, J. Phys. Chem. C 121 (2017) 13135–13143, http://dx.doi.org/10.1021/acs.jpcc.7b01990.
[48] M. Pourbaix, Atlas of Electrochemical Equilibria, second ed., National Association of Corrosion Engineers, Houston, 1974.